

# How to determine a dineutron correlation in Borromean nuclei via a quasi-free knockout ( $p, pn$ ) reaction?

Yuma Kikuchi,<sup>1</sup> Kazuyuki Ogata,<sup>2</sup> Yuki Kubota,<sup>1,3</sup> Masaki Sasano,<sup>1</sup> and Tomohiro Uesaka<sup>1</sup>

<sup>1</sup>*RIKEN Nishina Center, Wako 351-0198, Japan\**

<sup>2</sup>*Research Center for Nuclear Physics (RCNP),*

*Osaka University, Ibaraki 567-0047, Japan*

<sup>3</sup>*Center for Nuclear Study (CNS), The University of Tokyo, Tokyo 113-0001, Japan*

(Dated: December 3, 2024)

## Abstract

The quasi-free neutron knockout reaction on  ${}^6\text{He}$  is investigated to discuss the dineutron correlation in the ground state. In the present work, the momentum distributions of the two emitted neutrons are calculated with the  $\alpha + n + n$  three-body model and the simple reaction model, and the effects of the knockout process via the  ${}^5\text{He}$  resonance and the target dependence in the momentum distributions are discussed. From the calculation, it is found that a clear signature of the dineutron correlation can be obtained by choosing the kinematical condition to exclude the process via the  ${}^5\text{He}$  resonance, while the inclusion of the  ${}^5\text{He}$  resonance drastically changes the momentum distributions. It is also shown to be important to use the proton target in the quantitative discussion on the dineutron correlation by the knockout reaction. In addition to theoretical arguments, a possible experimental setup to determine the dineutron correlation via the quasi-free knockout reaction is considered.

---

\* yuma.kikuchi@riken.jp

## I. INTRODUCTION

A two-neutron halo structure observed in  ${}^6\text{He}$ ,  ${}^{11}\text{Li}$ , and so on is one of the most interesting topics in neutron-rich nuclei [1, 2]. Two-neutron halo nuclei are the Borromean systems, in which no binary subsystems have bound states, and have been extensively studied from both theoretical and experimental sides to understand their exotic binding mechanisms. Theoretically, two-neutron halo nuclei have been studied by using the core +  $n$  +  $n$  three-body models [3–12]. From the three-body model calculations, the importance of correlations between halo neutrons has been suggested in their bindings [3, 7]. It has been also shown that such a two-neutron correlation in the ground state is characterized as a spatially-correlated neutron pair, the so-called dineutron [3, 6, 8, 10].

In order to experimentally investigate the correlation between halo neutrons through the excitation mechanism of two-neutron halo nuclei, Coulomb breakup reactions have been employed [13–18]. The cross sections in the Coulomb breakup reactions are found to have a low-lying peak just above the breakup thresholds. This peak has been expected to be responsible to properties of weakly-bound halo neutrons. In addition, the cluster sum rule of the  $E1$  transition has been discussed to be useful to investigate the ground-state structure of the dineutron [19]. The Coulomb breakup reaction is dominated by the  $E1$  transition, and the  $E1$  transition strength is deduced from the Coulomb breakup cross section. The cluster sum rule value of the  $E1$  transition depends only on the geometrical configuration of halo neutrons in the ground state. Thus, the spatial correlation between halo neutrons has been discussed from the  $E1$  sum rule value. Actually, for the  ${}^{11}\text{Li}$  case, the opening angle between two halo neutrons was derived as  $48_{-18}^{+14}$  degrees from the observed Coulomb breakup cross section [18]. The observed opening angle indicates the spatial correlations of two halo neutrons.

In spite of the advantages, it is shown, from theoretical sides, that the Coulomb breakup reactions have uncertainties in extracting the information on the ground-state structure of two-neutron halo nuclei. Firstly, it is indicated that the low-lying peaks in the cross sections are governed by strong final-state interactions (FSIs) and the sequential decay via the core +  $n$  resonance dominates the low-lying peak [11, 12]. This fact shows that the geometrical configuration in the ground state cannot be extracted from the observables other than the cluster sum rule value. In addition, the cluster sum rule value itself has an

uncertainty coming from the excited components of the core nucleus in the ground state of two-neutron halo nuclei: In the cluster sum rule, the core nucleus is assumed to be inert. However, it is shown that in the  $^{11}\text{Li}$  case the sum rule value is reduced by about 15 % by taking into account the  $^9\text{Li}$  core excitation [12]. To discuss the ground-state structure such as the dineutron more quantitatively, other kinds of reactions are required.

The knockout reaction is another useful tool to investigate the ground-state structure of nuclei. In fact, for two-neutron halo nuclei  $^{11}\text{Li}$  and  $^{14}\text{Be}$ , the one-neutron knockout reaction was employed by bombarding them on the  $^9\text{Be}$  target, and contributions of S- and P-states were discussed by using the angular distributions of the emitted neutrons [20]. In the results of Ref. [20], the relative contributions of different partial waves in  $^{11}\text{Li}$  were determined by taking into account the interference between different parity partial waves, which appears as the asymmetry in the angular distribution. The interference between different parity waves is a key for the dineutron correlation, but the dineutron correlation was not discussed in Ref. [20]. It is interesting to discuss the dineutron correlation from the asymmetry in the angular distribution of the knocked-out neutron from the two-neutron halo nuclei.

The purpose of this work is to investigate a possibility to extract more quantitative and more reliable information of the dineutron correlation in Borromean nuclei by means of the proton-induced neutron knockout reaction. Throughout the paper,  $^6\text{He}$  is taken as an example, but the method presented here is applicable to any Borromean nuclei. In the one-neutron knockout reactions of two-neutron halo nuclei, the other halo neutron is immediately emitted because of the Borromean nature. We calculate the momentum distributions of two emitted neutrons, and discuss the spatial correlation between the neutrons. In particular, we calculate the distribution of the opening angle between the momentum vectors of the two emitted neutrons.

In discussing the spatial correlations, we consider the quasi-free condition to minimize the FSIs in the knockout reaction. In the quasi-free condition, the knocked-out neutron with high-momentum transfer is almost free from the FSIs, and hence, it carries out information on the ground-state structure. Furthermore, it is essential to use a probe which enables us to see the inner part of the two-neutron wave function to obtain a clear signature of the dineutron correlation from the knockout reaction. In this work, we show that a proton target is suitable for such a probe in contrast to heavy ions which makes the reaction much peripheral.

It is also important to minimize the effect of the knockout process via the  ${}^5\text{He}$  resonance to discuss the dineutron correlation in  ${}^6\text{He}$ . If the knockout reaction is dominated by the process via the  ${}^5\text{He}$  resonance, the opening angle distribution is governed by the  $3/2^-$  single-particle orbit corresponding to the  ${}^5\text{He}$  resonance. Such a dominance of the single spin-parity orbit suppresses the asymmetry in the distribution, because the asymmetry comes from the interference between different parity single-particle orbits. In this work, we estimate the effect of the process via the  ${}^5\text{He}$  resonance on the distributions, and try to find the kinematical condition to exclude the contribution from the knockout process via the  ${}^5\text{He}$  resonance.

In the last part, a possible experimental setup that suffices all the requirements placed by the theoretical arguments is considered. A high-momentum transfer, high statistics, and availability to pin down the state of the core are the keys.

This paper is organized as follows. In Sec. II, we briefly explain the  $\alpha + n + n$  three-body model for  ${}^6\text{He}$  and the calculation of the knockout reaction. Next, we show the calculated momentum distributions and discuss the effect of the knockout process via the  ${}^5\text{He}$  resonance and target dependence in the momentum distribution. From the calculated distributions, we show the possibility of direct measurement of dineutron in  ${}^6\text{He}$ . In addition to theoretical arguments, a possible experimental setup to determine the dineutron correlation via the quasi-free knockout reaction is considered. All the results and discussions are summarized in Sec. IV.

## II. MODEL

### A. $\alpha + n + n$ three-body model for ${}^6\text{He}$

Before discussing the knockout reaction, we explain the  $\alpha + n + n$  three-body model for  ${}^6\text{He}$  briefly. To solve the relative motion of the  $\alpha + n + n$  system, we employ the orthogonality condition model (OCM) [21].

In the  $\alpha + n + n$  OCM, the wave function for  ${}^6\text{He}$  is described as

$$\Phi_{6\text{He}} = \Phi_{\alpha}\chi_{nn}, \quad (1)$$

where the wave function of the  $\alpha$  core is expressed as  $\Phi_{\alpha}$ . The  $\alpha$  core is described by the harmonic oscillator wave functions for the  $(0s_{1/2})^4$  configuration, whose oscillator length  $b_c$

is taken as 1.4 fm to reproduce the observed charge radius of  ${}^4\text{He}$ .

The relative wave function of the  $\alpha + n + n$  system is obtained by solving the following Schrödinger equation;

$$\hat{H}\chi_{nn} = E\chi_{nn}. \quad (2)$$

The Schrödinger equation in Eq. (2) is accurately solved with a few-body technique. Here, we employ the variational method called the hybrid- $VT$  model whose detailed explanation is given in Ref. [7].

The total Hamiltonian in Eq. (2) is given by

$$\hat{H} = \sum_{i=1}^3 \hat{t}_i - \hat{T}_{\text{cm}} + \sum_{i=1}^2 \hat{V}_{\alpha n}(\boldsymbol{\xi}_i) + \hat{V}_{nn} + \hat{V}_{\text{PF}} + \hat{V}_{\alpha nn}, \quad (3)$$

where  $\hat{t}_i$  and  $\hat{T}_{\text{cm}}$  are kinetic operators for the  $i$ -th particle and the center-of-mass motion in the  $\alpha + n + n$  system, respectively. For two-body interactions for  $\alpha$ - $n$  and  $n$ - $n$ , we use the effective interactions which reproduce the scattering observables for each subsystems. We use the KKNN potential [22] for  $\hat{V}_{\alpha n}$ , where  $\boldsymbol{\xi}_i$  is the relative coordinate between the  $\alpha$  particle and the  $i$ -th neutron. For  $\hat{V}_{nn}$ , we use the Minnesota force [23] whose exchange parameter is taken as 0.95.

The Pauli principle between the  $\alpha$  core and neutrons is taken into account by the so-called pseudo potential  $\hat{V}_{\text{PF}}$ . The pseudo potential is a projection operator to remove the Pauli forbidden state  $\phi_{\text{PF}}$  from the relative motion between the  $\alpha$  and neutrons and is given by

$$\hat{V}_{\text{PF}} = \lambda |\phi_{\text{PF}}\rangle \langle \phi_{\text{PF}}|. \quad (4)$$

The Pauli forbidden state is defined as the  $0s$  orbits occupied by the  $\alpha$  core. The strength  $\lambda$  is taken as  $10^6$  MeV in the present calculation.

In the  $\alpha + n + n$  OCM, the ground state of  ${}^6\text{He}$  is slightly underbound by using only the two-body interactions. To reproduce the ground-state properties, we introduce the effective  $\alpha nn$  three-body interaction [11, 29], which is given by

$$\hat{V}_{\alpha nn} = V_3 e^{-\mu(\xi_1^2 + \xi_2^2)}, \quad (5)$$

where  $V_3$  and  $\mu$  are determined to reproduce the observed binding energy and matter radius of the  ${}^6\text{He}$  ground state. We here take  $V_3$  and  $\mu$  as  $-1.503$  MeV and  $0.07/b_c^2$  fm $^{-2}$ . The ground-state properties obtained with the three-body interaction is listed in TABLE. I.

TABLE I. Ground-state properties of  ${}^6\text{He}$ . The two-neutron separation energy,  $S_{2n}$ , and matter and charge radii,  $R_m$  and  $R_{\text{ch}}$ , are presented. The Probabilities of the partial wave components,  $P((l_j)^2)$ , in the relative coordinate set shown in Fig. 1 are also listed.

|                      | Present | Exp.                                                                  |
|----------------------|---------|-----------------------------------------------------------------------|
| $S_{2n}$ (MeV)       | 0.975   | 0.973 <sup>a</sup>                                                    |
| $R_m$ (fm)           | 2.46    | 2.48±0.03 <sup>b</sup><br>2.33±0.04 <sup>c</sup><br>2.50 <sup>d</sup> |
| $R_{\text{ch}}$ (fm) | 2.04    | 2.068(11) <sup>e</sup>                                                |
| $P((p_{3/2})^2)$     | 87.5 %  |                                                                       |
| $P((p_{1/2})^2)$     | 3.6 %   |                                                                       |
| $P((s_{1/2})^2)$     | 7.9 %   |                                                                       |
| $P((d_{5/2})^2)$     | 0.4 %   |                                                                       |
| $P((d_{3/2})^2)$     | 0.1 %   |                                                                       |
| $P((f_{7/2})^2)$     | 0.3 %   |                                                                       |
| $P((f_{5/2})^2)$     | 0.1 %   |                                                                       |

<sup>a</sup> Reference [24]

<sup>b</sup> Reference [25]

<sup>c</sup> Reference [26]

<sup>d</sup> Reference [27]

<sup>e</sup> Reference [28]

## B. One-neutron knockout cross section from ${}^6\text{He}$

We here consider the neutron knockout reaction on  ${}^6\text{He}$  by a proton target at 250 MeV/nucleon. The cross section for the  $(p,pn)$  reaction on  ${}^6\text{He}$  is given by

$$\frac{d^9\sigma}{d\mathbf{k}d\mathbf{K}d\mathbf{P}} \propto \frac{(2\pi)^4\mu_R}{\hbar^2 P_0} |\mathcal{T}_{\mathbf{P}_0}(\mathbf{k}, \mathbf{K}, \mathbf{P})|^2, \quad (6)$$

where  $P_0$  is the incident momentum of  ${}^6\text{He}$  the center-of-mass system and  $\mu_R$  is the reduced mass corresponding to the relative motion between the proton and  ${}^6\text{He}$ . The  $T$ -matrix in

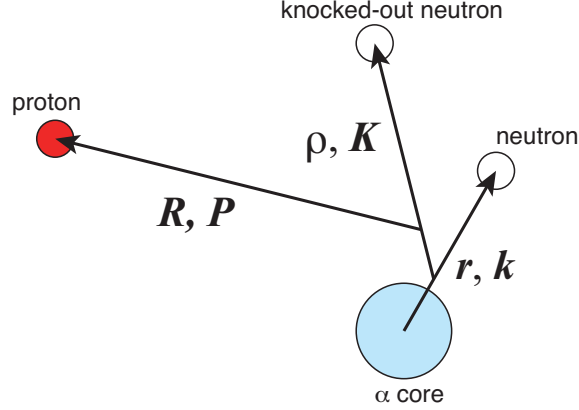


FIG. 1. (Color online) Relative coordinates and momenta employed in the present calculation.

Eq. (6) is defined as

$$\begin{aligned} \mathcal{T}_{\mathbf{P}_0}(\mathbf{k}, \mathbf{K}, \mathbf{P}) = & \left\langle \phi_0(\mathbf{P}, \mathbf{R}) \otimes \Psi_{6\text{He}}(\mathbf{k}, \mathbf{K}, \mathbf{r}, \boldsymbol{\rho}) \right| \\ & \times \hat{V}_f \left| \psi(\mathbf{P}_0, \mathbf{R}) \otimes \Phi_{\text{gs}}(\mathbf{r}, \boldsymbol{\rho}) \right\rangle \end{aligned} \quad (7)$$

in the post-form representation, where  $\phi_0$  is a plane wave between the target and projectile. The interaction in the final state,  $\hat{V}_f$ , is the sum of the interactions between proton and each constituent particle in  ${}^6\text{He}$ . The wave functions of  ${}^6\text{He}$  in the initial ground state and the final scattering one is represented by  $\Phi_{\text{gs}}$  and  $\Psi_{6\text{He}}$ , respectively. The initial scattering wave between the target and projectile is given by  $\psi$ . The relative coordinates and momenta in Eqs. (6) and (7) are defined as shown in Fig. 1.

In the present calculation, we use the simple reaction model, in which the knockout process via the  ${}^5\text{He}$  resonance and the absorption effect by the target nucleus are taken into account. We approximately describe the initial scattering wave  $\psi$  as

$$\psi(\mathbf{P}_0, \mathbf{R}) = D(\mathbf{R})e^{i\mathbf{P}_0 \cdot \mathbf{R}}, \quad (8)$$

where  $D(\mathbf{R})$  is the dumping factor coming from the absorption by the proton target and is calculated with the eikonal approximation. Furthermore, we take into account only the  $p$ - $n$  interaction as a residual interaction for the neutron knockout by a proton target, and hence, the other interactions in  $\hat{V}_f$  are operated on the wave function in the final state  $\phi_0$ . Operating these interactions on the final-state wave function,  $\phi_0$  is transformed as

$$\phi_0(\mathbf{P}, \mathbf{R}) \rightarrow \psi'(\mathbf{P}, \mathbf{R}) = D'(\mathbf{R})e^{i\mathbf{P} \cdot \mathbf{R}}, \quad (9)$$

where  $D'(\mathbf{R})$  is calculated in similar to that in the initial state.

When we employ the zero-range interaction for the  $p$ - $n$  one, we obtain the  $T$ -matrix in Eq. (7) as

$$\mathcal{T}_{\mathbf{P}_0}(\mathbf{k}, \mathbf{K}, \mathbf{P}) = V_0 \left\langle \Psi_{6\text{He}}(\mathbf{k}, \mathbf{K}, \mathbf{r}, \boldsymbol{\rho}) \left| \tilde{D}(\boldsymbol{\rho}) e^{i\mathbf{q}\cdot\boldsymbol{\rho}} \right| \Phi_{\text{gs}}(\mathbf{r}, \boldsymbol{\rho}) \right\rangle, \quad (10)$$

where  $V_0$  is the strength of the  $p$ - $n$  interaction and  $\mathbf{q}$  is related to the transferred momentum as  $\mathbf{q} = 5(\mathbf{P}_0 - \mathbf{P})/6$ . The dumping factor  $\tilde{D}(\boldsymbol{\rho})$  in Eq. (10) is given by

$$\tilde{D}(\boldsymbol{\rho}) = D \left( \frac{5}{6}\boldsymbol{\rho} \right) \cdot D' \left( \frac{5}{6}\boldsymbol{\rho} \right). \quad (11)$$

Considering the quasi-free condition, we describe the scattering wave function of  ${}^6\text{He}$ ,  $\Psi_{6\text{He}}$ , as

$$\Psi_{6\text{He}}(\mathbf{k}, \mathbf{K}, \mathbf{r}, \boldsymbol{\rho}) = \psi_{\alpha-n}(\mathbf{k}, \mathbf{r}) \otimes e^{i\mathbf{K}\cdot\boldsymbol{\rho}}. \quad (12)$$

The relative motion between the knocked-out neutron and the rest is described by a plane wave since the knocked-out neutron is free from the FSIs in the quasi-free condition. The  ${}^5\text{He}$  residue is expressed by the exact scattering wave function of  $\alpha + n$ ,  $\psi_{\alpha-n}$ , to take into account the process via the  ${}^5\text{He}$  resonance in the knockout reaction. The wave function  $\psi_{\alpha-n}$  is solved with the same  $\alpha$ - $n$  interaction as used in Eq. (3). By combining Eqs. (10) and (12), we obtain

$$\mathcal{T}_{\mathbf{P}_0}(\mathbf{k}, \mathbf{K}, \mathbf{P}) = V_0 \left\langle \psi_{\alpha-n}(\mathbf{k}, \mathbf{r}) \otimes e^{i\mathbf{K}\cdot\boldsymbol{\rho}} \left| \tilde{D}(\boldsymbol{\rho}) e^{i\mathbf{q}\cdot\boldsymbol{\rho}} \right| \Phi_{\text{gs}}(\mathbf{r}, \boldsymbol{\rho}) \right\rangle. \quad (13)$$

From Eq. (13), we also define the following  $T$ -matrix;

$$\begin{aligned} \mathcal{T}(\mathbf{k}, \mathbf{K}') &= \iint d\mathbf{K} d\mathbf{P} \mathcal{T}_{\mathbf{P}_0}(\mathbf{k}, \mathbf{K}, \mathbf{P}) \delta(\mathbf{K}' - \mathbf{K} + \mathbf{q}) \\ &= V_0 \left\langle \psi_{\alpha-n}(\mathbf{k}, \mathbf{r}) \otimes e^{i\mathbf{K}'\cdot\boldsymbol{\rho}} \left| \tilde{D}(\boldsymbol{\rho}) \right| \Phi_{\text{gs}}(\mathbf{r}, \boldsymbol{\rho}) \right\rangle, \end{aligned} \quad (14)$$

where  $\mathbf{K}' = \mathbf{K} - \mathbf{q}$ .

Using Eqs. (6) and (14), we obtain the double-differential cross section as

$$\frac{d^2\sigma}{dk_{\alpha-n}d\theta} \propto \frac{(2\pi)^4 \mu_R}{\hbar^2 P_0} \cdot V_0^2 \cdot \frac{d^2W}{dk_{\alpha-n}d\theta}, \quad (15)$$

where  $k_{\alpha-n}$  is a relative momentum between the  $\alpha$  particle and the neutron in the  ${}^5\text{He}$  residue and  $\theta$  is opening angle between two momenta  $\mathbf{k}$  and  $\mathbf{K}$ . In the present analysis, we calculate  $d^2W/dk_{\alpha-n}d\theta$  to discuss the spatial correlation between halo neutrons in  ${}^6\text{He}$ . The two-dimensional momentum distribution  $d^2W/dk_{\alpha-n}d\theta$  is defined as

$$\begin{aligned} \frac{d^2W}{dk_{\alpha-n}d\theta} &= \iint d\mathbf{k} d\mathbf{K}' \delta(k - k_{\alpha-n}) \delta(\theta' - \theta) \\ &\quad \times \left| \left\langle \psi_{\alpha-n}(\mathbf{k}, \mathbf{r}) \otimes e^{i\mathbf{K}'\cdot\boldsymbol{\rho}} \left| \tilde{D}(\boldsymbol{\rho}) \right| \Phi_{\text{gs}}(\mathbf{r}, \boldsymbol{\rho}) \right\rangle \right|^2, \end{aligned} \quad (16)$$

where  $\cos \theta' = \hat{\mathbf{k}} \cdot \hat{\mathbf{K}}'$ . This distribution gives

$$\iint \frac{d^2W}{dk_{\alpha-n}d\theta} dk_{\alpha-n}d\theta = 1 \quad (17)$$

when  $\tilde{D}(\boldsymbol{\rho}) = 1$ . We also define the opening angle distribution for two emitted neutrons by integrating Eq. (16) over  $k_{\alpha-n}$  as

$$\frac{dW}{d\theta} = \int \frac{d^2W}{dk_{\alpha-n}d\theta} dk_{\alpha-n}. \quad (18)$$

### III. RESULTS

#### A. Dineutron correlation in the ground state

Before discussing the momentum distribution in the knockout reaction, we first show the momentum distribution of the ground state of  ${}^6\text{He}$  to see the dineutron correlation in the momentum space. The ground-state momentum distribution is calculated by taking the dumping factor  $\tilde{D}(\boldsymbol{\rho})$  as unity and switching off the  $\alpha$ - $n$  interaction in the final states. We thus replace the scattering wave function of  $\alpha + n$ ,  $\psi_{\alpha-n}(\mathbf{k}, \mathbf{r})$ , with the plane wave  $e^{i\mathbf{k}\cdot\mathbf{r}}$  in Eq. (14).

The calculated momentum distribution is shown in Fig. 2. From the definition of the momentum distribution in Eq. (16), the distribution shown in Fig. 2 is nothing but the Fourier-transformed ground-state wave function of  ${}^6\text{He}$ . One sees that the momentum distribution in Fig. 2 has a two-peaked structure and the strength at around  $(k_{\alpha-n}, \theta) = (0.4 \text{ fm}^{-1}, 135 \text{ degrees})$  is enhanced compared to the other peak. This enhancement is clearly understood to come from the dineutron correlation in the ground state of  ${}^6\text{He}$ .

This dineutron correlation in the momentum space is also seen in the opening angle distribution. We calculate the  $dW/d\theta$  given by Eq. (18) with switching off the  $\alpha$ - $n$  interaction in the final state and taking the dumping factor as unity. The result is shown in Fig. 3. The distribution in Fig. 3 has a two-peaked structure as expected from the result in Fig. 2. The peak at  $\theta > 90$  degrees, corresponding to the dineutron correlation is slightly higher than that to the cigar-like one at  $\theta < 90$  degrees.

The dineutron correlation seen in the opening angle distribution of Fig. 3 is found more clearly in the momentum distributions with the fixed relative momentum for  $\alpha + n$ ,  $k_{\alpha-n}$ . In Fig. 4, we show the momentum distribution with the fixed values of  $k_{\alpha-n}$ . Here, we choose

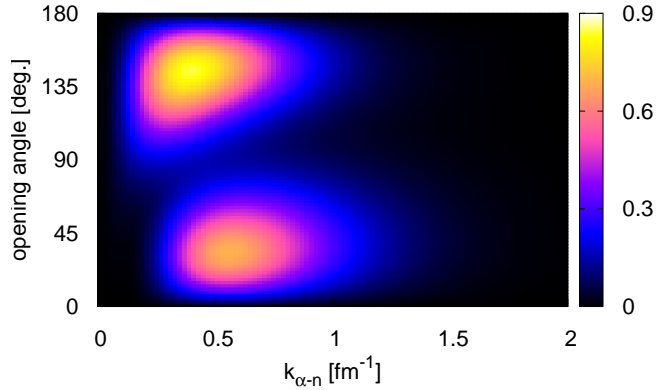


FIG. 2. (Color online) Two-dimensional momentum distribution of the halo neutrons in the ground state of  ${}^6\text{He}$ .

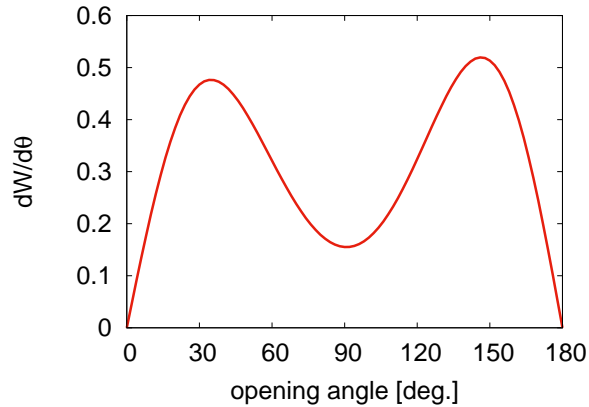


FIG. 3. (Color online) Opening angle distribution of the halo neutrons.

two momenta:  $k_{\alpha-n} = 0.2$  and  $1.0 \text{ fm}^{-1}$ . At  $k_{\alpha-n} = 0.2 \text{ fm}^{-1}$ , one sees that the significant enhancement at larger angles corresponding to the dineutron correlation, while the distribution at  $k_{\alpha-n} = 1.0 \text{ fm}^{-1}$  shows the enhancement at smaller opening angle corresponding to the cigar-like configuration. This result shows that the dineutron correlation in the ground state is developed in the surface region of  ${}^6\text{He}$ , which corresponds to small momentum between the  $\alpha$  core and neutron.

In our calculation, the asymmetry in the distributions in Fig. 4 dominantly comes from the interference between the  $(0p_{3/2})^2$  and  $(1s_{1/2})^2$  components. In the ground state of  ${}^6\text{He}$ , the relative phase between  $(0p_{3/2})^2$  and  $(1s_{1/2})^2$  is changed as  $k_{\alpha-n} \sim 0.5 \text{ fm}^{-1}$  due to the fact that the single-particle wave function of  $1s_{1/2}$  has a node at  $k_{\alpha-n} \sim 0.5 \text{ fm}^{-1}$ . This change in

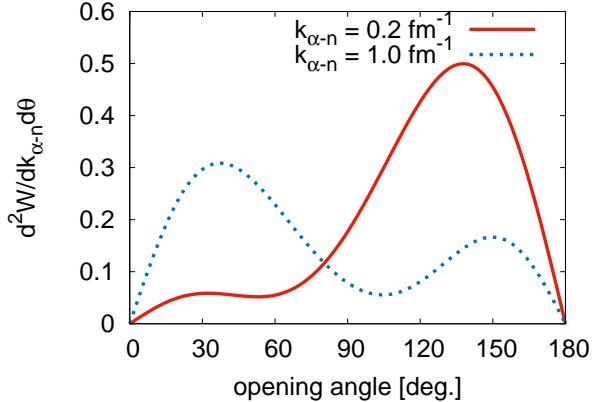


FIG. 4. (Color online) Ground-state momentum distributions of the halo neutrons with fixed  $k_{\alpha-n}$ . The red (solid) and blue (dotted) lines represent the distributions for  $k_{\alpha-n} = 0.2$  and  $1.0 \text{ fm}^{-1}$ , respectively.

the relative phase makes the interference patterns at  $k_{\alpha-n} = 0.2$  and  $1.0 \text{ fm}^{-1}$  different from each other.

### B. Effect of knockout process via the ${}^5\text{He}$ resonance

To investigate the effect of the process via the  ${}^5\text{He}$  resonance on the momentum distribution in the knockout reaction, we switch on the  $\alpha$ - $n$  interaction in the final states, and calculate the momentum distribution. Here, we focus our discussion on the effect of the process via the  ${}^5\text{He}$  resonance, and the absorption in the knockout reaction is neglected by taking the dumping factor in Eq. (10) as  $\tilde{D}(\boldsymbol{\rho}) = 1$ .

The calculated momentum distribution is shown in Fig. 5. We see that the inclusion of the  ${}^5\text{He}$  resonance changes the distribution drastically, compared to the result in Fig. 3. The distribution is concentrated on the  $k_{\alpha-n} \sim 0.2 \text{ fm}^{-1}$  region and has symmetric two-peaked structure with respect to  $\theta = 90$  degrees. This shape of the distribution shows that the knockout reaction of  ${}^6\text{He}$  is dominated by the process via the  ${}^5\text{He}(3/2^-)$  resonance. The resonance energy of  ${}^5\text{He}(3/2^-)$  is coincident with  $k_{\alpha-n} \sim 0.2 \text{ fm}^{-1}$  and the symmetric two-peaked structure comes from the  $(p_{3/2})^2$  configuration of the two emitted neutrons, which is favored by the process via the  ${}^5\text{He}$  resonance.

Furthermore, in the opening angle distribution shown in Fig. 6, we cannot find any signature of the enhancement of the dineutron correlation. By including the process via the

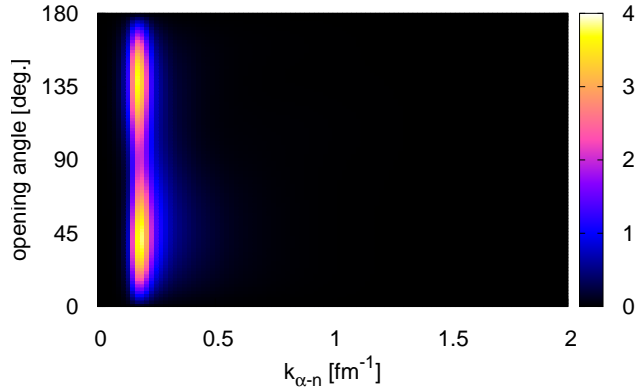


FIG. 5. (Color online) Two-dimensional momentum distribution of the emitted neutrons in the knockout reaction.

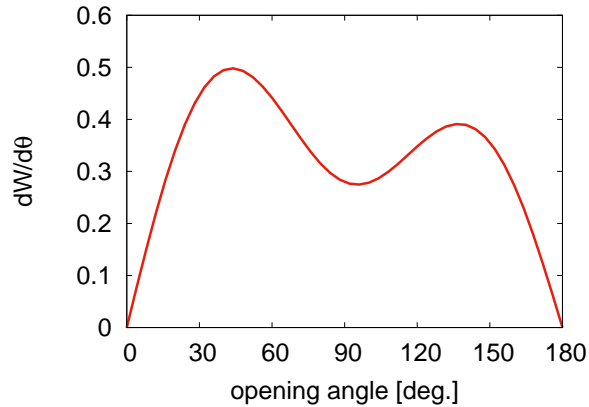


FIG. 6. (Color online) Opening angle distribution of the emitted neutrons in the knockout reaction.

${}^5\text{He}$  resonance, the distribution is changed to have the largest peak at  $\theta < 90$  degrees and the contribution from the dineutron correlation becomes smaller than that from the cigar-like one.

From the results in Figs. 5 and 6, it is shown that the inclusion of the  ${}^5\text{He}$  resonance drastically changes the distributions and disturbs to find the signature of the dineutron correlation from the knockout reaction of  ${}^6\text{He}$ . To clarify the signature of the dineutron correlation in the knockout reaction of  ${}^6\text{He}$ , it is important to minimize the effect of the process via the  ${}^5\text{He}$  resonance on the momentum distribution.

For this purpose, we calculate the distributions by fixing the relative momentum between the  $\alpha + n$ . Here, we choose the off-resonant relative momentum for the  $\alpha + n$  subsystem.

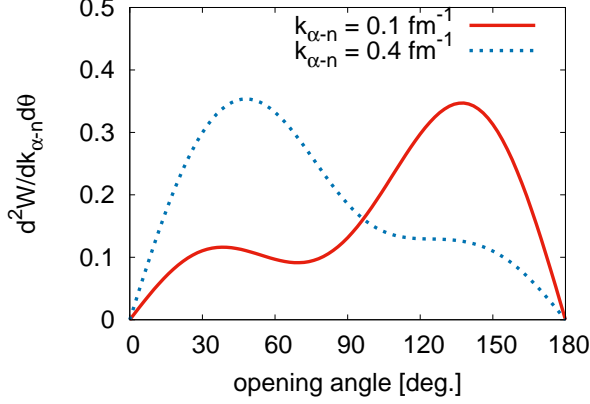


FIG. 7. (Color online) Momentum distributions of the emitted neutrons in the knockout reaction with fixed  $k_{\alpha-n}$ . The red (solid) and blue (dotted) lines represent the distributions for  $k_{\alpha-n} = 0.1$  and  $0.4 \text{ fm}^{-1}$ , respectively.

The angular distributions calculated with  $k_{\alpha-n} = 0.1$  and  $0.4 \text{ fm}^{-1}$ , which are respectively smaller and larger than the  $\alpha$ - $n$  relative momentum corresponding to  ${}^5\text{He}(3/2^-)$  resonance, are shown in Fig. 7. The patterns of the distributions are similar to those in Fig. 4. For the smaller momentum,  $k_{\alpha-n} = 0.1 \text{ fm}^{-1}$ , the distribution shows a clear signature of the dineutron correlation at  $\theta > 90$  degrees, while the distribution for the larger momentum,  $k_{\alpha-n} = 0.4 \text{ fm}^{-1}$ , shows the cigar-like peak.

The results in Fig. 7 show that the information on the spatial correlation in the  ${}^6\text{He}$  ground state survives in the quasi-free neutron-knockout reaction by choosing the kinematical condition to exclude the knockout process via the  ${}^5\text{He}$  resonance. The asymmetric pattern in the momentum distribution is clearly confirmed by fixing  $k_{\alpha-n}$  even if the knockout process via the  ${}^5\text{He}$  resonance dominates the neutron-knockout reaction of  ${}^6\text{He}$ . On the other hand, the opening angle distribution calculated by integrating over  $k_{\alpha-n}$  is not helpful to investigate the spatial correlation such as dineutron.

### C. Effect of the absorption by the target nucleus on the momentum distributions

We estimate the effect of the absorption by the target nucleus on the momentum distributions. First, we show the dumping factor used in the present calculation. In Fig. 8, the dumping factor for the proton target, given in Eq. (11), is shown in comparison with that for the  ${}^{12}\text{C}$  target for reference. From the results in Fig. 8, we see that the proton target is

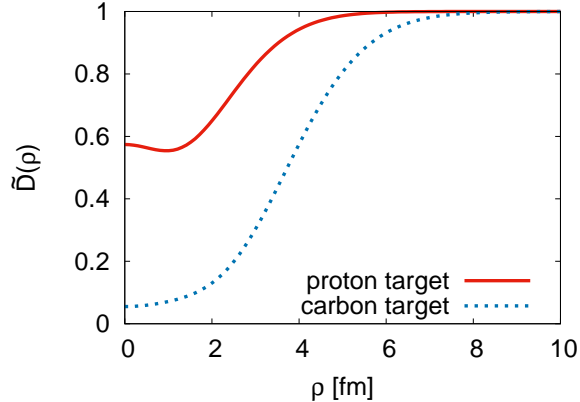


FIG. 8. (Color online) Dumping factor for the neutron-knockout reaction on  ${}^6\text{He}$  by a proton target at 250 MeV/nucleon, shown as red (solid) line. For reference, that by a  ${}^{12}\text{C}$  target is also shown as blue (dotted) line.

much more transparent than the  ${}^{12}\text{C}$  one. The dumping factor for the proton target gives 0.57 at the origin while that for  ${}^{12}\text{C}$  target gives only 0.06.

Using the dumping factors shown in Fig. 8, we calculate the momentum distributions with fixed values of  $k_{\alpha-n}$ . Here, to see the target-dependence of the momentum distributions, we calculate the distributions not only for the proton target but also for the  ${}^{12}\text{C}$  one. In Figs. 9 and 10, we show the calculated distributions for  $k_{\alpha-n} = 0.1$  and  $0.4 \text{ fm}^{-1}$ , respectively, in comparison with the distributions without the dumping factor. The absorptions by the target nuclei reduce the strengths of momentum distributions both at  $k_{\alpha-n} = 0.1$  and  $0.4 \text{ fm}^{-1}$ . It is also seen that the absorptions are stronger at higher  $k_{\alpha-n}$ , which corresponds to the interior region of the two-neutron wave function, and the reduction of the strength at higher  $k_{\alpha-n}$  is much serious for the  ${}^{12}\text{C}$  case. For  $k_{\alpha-n} = 0.4 \text{ fm}^{-1}$ , the strength at the peak position for  ${}^{12}\text{C}$  is 7.37 times smaller than the case without absorption, while that for the proton is 1.72 times smaller than that. These trends are naturally understood by the shapes of the dumping factors shown in Fig. 8.

Furthermore, as seen in Figs. 9 and 10, the asymmetry in the momentum distributions is suppressed as the absorption becomes stronger. This fact indicates that the use of the proton target is essential to investigate the spatial correlation of halo neutrons in the quasi-free knockout reactions. To determine the asymmetry in the momentum distributions of the two emitted neutrons quantitatively, the transparent target such as a proton provides us with

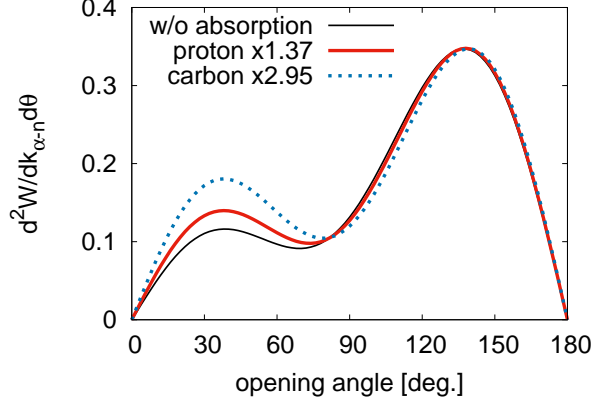


FIG. 9. (Color online) Momentum distributions of the emitted neutrons with distortion effects for  $k_{\alpha-n} = 0.1 \text{ fm}^{-1}$ . The red (solid) and blue (dotted) lines represent the distributions of the knockout reactions by the proton and  $^{12}\text{C}$  targets, respectively. The black thin line is the distributions without the absorption. The distributions for the proton and carbon targets are multiplied by the factors, which are indicated in keys, to adjust the magnitude of the largest peak in the distribution without absorption.

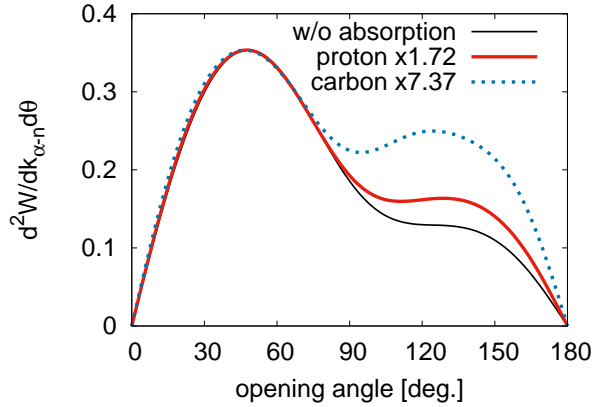


FIG. 10. (Color online) Same as Fig. 9 but for  $k_{\alpha-n} = 0.4 \text{ fm}^{-1}$ .

clean data, while the heavier target having a large absorption could mask the asymmetry in the distributions and makes the experimental statistics low.

#### D. Experimental approaches to the two-neutron correlation

We have clarified advantages of the proton-induced neutron knockout reaction in investigation of two-neutron correlations in Borromean nuclei. The experimental extraction of

signatures of the two-neutron correlation discussed above demands (i) selection of the  $(p, pn)$  events with a sufficiently large momentum transfer, (ii) high statistics to divide the opening angle distribution according to  $k_{\alpha-n}$ , and (iii) a kinematically complete measurement to tag contribution from the excited core states. In the following, an inverse kinematics experiment with a hydrogen target is considered. A recoil proton and a knocked-out neutron are detected dedicated detectors placed sideways. A decay neutron and a residual ion after the  $(p, pn)$  reaction are analyzed with a large acceptance magnetic spectrometer, such as the SAMURAI [30] at RIBF and the ALADIN at GSI, equipped with high-efficiency neutron detector arrays.

In order to suppress possible effects of three-body FSIs, momenta of the recoil proton and the knocked-out neutron should be sufficiently larger than nucleon Fermi momentum in a nucleus which is about  $1.3 \text{ fm}^{-1}$ . This condition can be fulfilled by using beams with incident energies higher than  $200 \text{ MeV/nucleon}$  and by restricting the recoil proton energy to be higher than  $80 \text{ MeV}$ . Radioactive nuclear beams at more than  $200 \text{ MeV/nucleon}$  are available at the RI Beam Factory in Japan and the GSI in Germany at present and at the FRIB in USA in near future.

Selection of the high-momentum transfer condition necessarily accompanies a small cross section. The proton-neutron elastic scattering cross section in the energy and momentum transfer regions considered is about  $0.5 \text{ mb/sr}$  while it is considerably large at forward angles. In order to obtain sufficient statistics in an momentum distribution at each  $k_{\alpha-n}$  for the small cross section, the experiment demands unprecedentedly high luminosity, typically, of  $10^{29} \text{ cm}^{-2}\text{sec}^{-1}$ . This can be realized with high-intensity radioactive nuclear beams with an intensity of  $10^{5-6} \text{ sec}^{-1}$  and a thick liquid hydrogen target with a thickness of  $10^{23-24} \text{ cm}^{-2}$ . An example of the latter is the MINOS[31]: The MINOS is a device consisting of a very thick liquid hydrogen target and a time projection chamber surrounding the target. The target thickness can be changeable and as much as  $10^{24} \text{ cm}^{-2}$ . Determination of the vertex position with the time projection chamber allows one to correct the energy loss of the beam and the residual ions in the target and thus to enable high luminosity experiments without a significant loss of experimental resolutions.

The high luminosity enables tagging of the excited core contribution in the Borromean nuclei. Effects of unbound core states, which are considered to be significant in  $^{11}\text{Li}$ , can be explored with an invariant mass spectroscopy of the excited core states. On the other hand,

those of bound excited core states, being more important in heavier Borromean nuclei, can be tagged through  $\gamma$ -ray detection with a high-efficiency scintillator array. New data on the effects of excited cores should reveal unexplored aspects of Borromean nuclei and bring about a better understanding of the two-neutron correlation in the nuclei.

#### IV. SUMMARY

We here investigated the dineutron correlation in  ${}^6\text{He}$  by using the quasi-free neutron knockout reaction. In the present analysis, we calculated the momentum distributions of two emitted neutrons, and compared them with those in the ground state to discuss the spatial correlation between halo neutrons. The calculated momentum distributions show the different patterns from the ground-state distributions due to the knockout process via the  ${}^5\text{He}(3/2^-)$  resonance. To minimize the effect of the process via the  ${}^5\text{He}$  resonance on the momentum distributions, we have also shown the momentum distributions by choosing the off-resonance region for the  $\alpha$ - $n$  relative momentum. By selecting  $\alpha$ - $n$  relative momentum to exclude the process via the  ${}^5\text{He}$  resonance, the distributions show similar patterns to the ground-state ones. For the lower  $\alpha$ - $n$  relative momentum, the calculated distribution shows a clear enhancement at larger opening angle between the momenta of the two emitted neutrons. This result suggests the spatially-correlated neutron pair at surface region of the halo nucleus  ${}^6\text{He}$ . In addition, we discussed the effect of the absorption by the target nucleus on the momentum distributions. From the calculation, it is shown that the absorption by the target reduces not only the magnitude of the momentum distribution but also asymmetry in the distribution. Our results indicate that the use of the proton target, which is the most transparent probe sensitive to neutrons, is essential to investigate the spatial correlation of halo neutrons. Furthermore, we also discuss a possible experimental setup to suffice all the requirements placed by the theoretical arguments.

## ACKNOWLEDGMENTS

This work was supported by a Grant-in-Aid from the Japan Society for the Promotion of Science (No. 25400255).

---

- [1] I. Tanihata, H. Hamagaki, O. Hashimoto, Y. Shida, N. Yoshikawa, K. Sugimoto, O. Yamakawa, T. Kobayashi, and N. Takahashi, *Phys. Rev. Lett.* **55**, 2676 (1985).
- [2] I. Tanihata, H. Savajols, and R. Kanungo, *Prog. Part. Nucl. Phys.* **68**, 215 (2013).
- [3] M. V. Zhukov, B. V. Danilin, D. V. Fedorov, J. M. Bang, I. J. Thompson, and J. S. Vaagen, *Phys. Rep.* **231**, 151 (1993).
- [4] A. Csóto, *Phys. Rev. C* **49**, 3035 (1994).
- [5] Y. Suzuki, *Nucl. Phys. A* **528**, 395 (1991).
- [6] S. Funada, H. Kameyama, and Y. Sakuragi, *Nucl. Phys. A* **575**, 93 (1994).
- [7] S. Aoyama, S. Mukai, K. Katō, and K. Ikeda, *Prog. Theor. Phys.* **93**, 99 (1995).
- [8] K. Hagino and H. Sagawa, *Phys. Rev. C* **72**, 044321 (2005).
- [9] T. Myo, K. Katō, S. Aoyama, and K. Ikeda, *Phys. Rev. C* **63**, 054313 (2001).
- [10] T. Myo, Y. Kikuchi, K. Katō, H. Toki, and K. Ikeda, *Prog. Theor. Phys.* **119**, 561 (2008).
- [11] Y. Kikuchi, K. Katō, T. Myo, M. Takashina, and K. Ikeda, *Phys. Rev. C* **81**, 044308 (2010).
- [12] Y. Kikuchi, T. Myo, K. Katō, and K. Ikeda, *Phys. Rev. C* **87**, 034606 (2013).
- [13] T. Aumann, D. Aleksandrov, L. Axelsson, T. Baumann, M. J. G. Borge, L. V. Chulkov, J. Cub, W. Dostal, B. Eberlein, T. W. Elze, *et al.*, *Phys. Rev. C* **59**, 1252 (1999).
- [14] J. Wang, A. Galonsky, J. J. Kruse, E. Tryggestad, R. H. White-Stevens, P. D. Zecher, Y. Iwata, K. Ieki, A. Horváth, F. Deák, *et al.*, *Phys. Rev. C* **65**, 034306 (2002).
- [15] K. Ieki, D. Sackett, A. Galonsky, C. A. Bertulani, J. J. Kruse, W. G. Lynch, D. J. Morrissey, N. A. Orr, H. Schulz, B. M. Sherrill, *et al.*, *Phys. Rev. Lett.* **70**, 730 (1993).
- [16] S. Shimoura, T. Nakamura, M. Ishihara, N. Inabe, T. Kobayashi, T. Kubo, R. H. Siemssen, I. Tanihata, and Y. Watanabe, *Phys. Lett. B* **348**, 29 (1995).
- [17] M. Zinser, F. Humbert, T. Nilsson, W. Schwab, H. Simon, T. Aumann, M. J. G. Borge, L. V. Chulkov, J. Cub, T. W. Elze, *et al.*, *Nucl. Phys. A* **619**, 151 (1997).

- [18] T. Nakamura, A. M. Vinodkumar, T. Sugimoto, N. Aoi, H. Baba, D. Bazin, N. Fukuda, T. Gomi, H. Hasegawa, N. Imai, *et al.*, Phys. Rev. Lett. **96**, 252502 (2006).
- [19] H. Esbensen and G. F. Bertsch, Nucl. Phys. A **542**, 310 (1992).
- [20] H. Simon, M. Meister, T. Aumann, M. Borge, L. Chulkov, U. D. Pramanik, T. Elze, H. Emling, C. Forssén, H. Geissel, *et al.*, Nuclear Physics A **791**, 267 (2007).
- [21] S. Saito, Prog. Theor. Phys. Suppl. **62**, 11 (1977).
- [22] H. Kanada, T. Kaneko, S. Nagata, and M. Nomoto, Prog. Theor. Phys. **61**, 1327 (1979).
- [23] D. R. Thompson, M. Lemere, and Y. C. Tang, Nucl. Phys. A **286**, 53 (1977).
- [24] D. R. Tilley, C. M. Cheves, J. L. Godwin, G. M. Hale, H. M. Hofmann, J. H. Kelley, C. G. Sheu, and H. R. Weller, Nucl. Phys. A **708**, 3 (2002).
- [25] I. Tanihata, T. Kobayashi, O. Yamakawa, S. Shimoura, K. Ekuni, K. Sugimoto, N. Takahashi, T. Shimoda, and H. Sato, Phys. Lett. B **206**, 592 (1988).
- [26] I. Tanihata, D. Hirata, T. Kobayashi, S. Shimoura, K. Sugimoto, and H. Toki, Phys. Lett. B **289**, 261 (1992).
- [27] J. S. Al-Khalili and J. A. Tostevin, Phys. Rev. C **57**, 1846 (1998).
- [28] P. Mueller, I. A. Sulai, A. C. C. Villari, J. A. Alcántara-Núñez, R. Alves-Condé, K. Bailey, G. W. F. Drake, M. Dubois, C. Eléon, G. Gaubert, *et al.*, Phys. Rev. Lett. **99**, 252501 (2007).
- [29] T. Myo, S. Aoyama, K. Katō, and K. Ikeda, Phys. Lett. B **576**, 281 (2003).
- [30] T. Kobayashi, N. Chiga, T. Isobe, Y. Kondo, T. Kubo, K. Kusaka, T. Motobayashi, T. Nakamura, J. Ohnishi, H. Okuno, *et al.*, Nucl. Instr. Meth. B **317**, 294 (2013).
- [31] A. Obertelli, A. Delbart, S. Anvar, L. Audirac, G. Authelet, H. Baba, B. Bruyneel, D. Calvet, F. Château, A. Corsi, *et al.*, Eur. Phys. J. A **50**, 8 (2014).